Astron. Astrophys. 332, 849–856 (1998)

ASTRONOMY AND ASTROPHYSICS

# The Chamaeleon infrared nebula revisited

## Infrared imaging and spectroscopy of a young stellar object⋆,⋆⋆

**Markus Feldt**[1], **Thomas Henning**[1], **Pierre O. Lagage**[3], **Volker Manske**[1], **Katharina Schreyer**[1], **and Bringfried Stecklum**[2]

[1] Astrophysikalisches Institut und Universitäts-Sternwarte, Schillergäßchen 2-3, D-07745 Jena, Germany
[2] Thüringer Landessternwarte Tautenburg, Sternwarte 5, D-07778 Tautenburg, Germany
[3] Centre d' Etude de Saclay, F-91191 Gif-sur-Yvette Cedex, France

Received 23 September 1997 / Accepted 17 December 1997

**Abstract.** We are presenting spectroscopic and imaging data on the Chamaeleon Infrared Nebula (Cha IRN). Imaging was done between 1 and 2.5 $\mu$m and at 10 $\mu$m. Spectra of the object were obtained in the 2.1 $\mu$m – 4.6 $\mu$m range by ground-based measurements as well as using ISOPHOT-S in the 2.5 $\mu$m – 11.6 $\mu$m range. By combining these data with a K-band speckle image and IRAS-LRS data, we draw a complete picture of the source. The system's geometry, consisting of central source, disk, and bipolar outflow cavities, is determined directly from the observational data. Thereby we confirm earlier assumptions on the basic geometry of the system as well as support newer speculations by Gledhill et al. (1996) about the presence of a binary system inside the Cha IRN.

Additionally, we fit a radiative transfer model to the spectral energy distribution and derive the dust composition from the ISOPHOT spectra and give the resulting abundance ratios. The spectroscopic data point to an unusually silicate-poor environment of this young stellar object or a special geometric arrangement which leads to a suppression of the feature. They also indicate one of the most prominent $H_2O$ ice features known as well as the presence of CO, $CO_2$, and possibly $NH_3$ ice.

**Key words:** stars: formation – ISM: jets and outflows – accretion, accretion disks – line: identification – radiative transfer

### 1. Introduction

The Chamaeleon Infrared Nebula (Cha IRN) is a bipolar reflection nebula in the Cha I dark cloud (Schwartz & Henize 1983). The source is associated with IRAS 11072-7727. In the near infrared, the typical appearance of a bipolar nebula with the two lobes separated by a dark plane points to the presence of a circumstellar disk. Cohen & Schwartz (1984) performed far-infrared measurements on Cha IRN, which revealed an elongated structure in north-south direction at 52 $\mu$m and 100 $\mu$m, ascribed to the coolest outer parts of the disk. They estimated the visual extinction towards the central object as $A_V \approx 10$ mag, the object itself being assumed to be either an A7 main sequence dwarf or a T Tauri star of photospheric type K7. From fitting a 65K blackbody to the spectral energy distribution (SED) and thereby determining the emitting area, they concluded that the disk possesses a major axis of 20″ (∼2800 AU at a distance of 140 pc after Rydgren 1980) and is viewed almost edge-on at an inclination of 88.5°. The new HIPPARCOS data on optically visible stars near Cha IRN suggest that the actual distance is closer to 190 pc. This distance is adopted throughout the paper.

Ageorges et al. (1996) performed a high-resolution polarization study in the near infrared (NIR) and concluded that Cha IRN consists of a central object surrounded by a disk with a radius of $r_d = 1000$ AU and a thickness of $z_d = 300$ AU, which is inclined by $70° \pm 6°$, assuming a distance of 140 pc. Their model for the circumstellar environment consists of a combination of a Toomre-like disk, a free-falling spherical envelope, and a bipolar cavity. The assumption concerning the central object was that of a star with $T_{\rm eff} = 7000$ K and $L = 18.1\,L_\odot$. However, aiming more at the determination of the geometry of the system, they fitted the polarization maps solely at one single wavelength. As intensity variations across the spectrum are disregarded by this procedure, the nature of the central object is not very well constrained.

Gledhill et al. (1996) argue from a tilt between the bipolar nebula axis and the polar axis of the disk as concluded from the polarization pattern that the system must possess two disks with a tilt of $\approx 15°$ with respect to each other. The dense inner disk would then be responsible for a highly non-isotropic illumination of the outer molecular disk and the outflow and thus provide the polarization. They suggest the tilt to be caused by tidal forces from a young binary system inside. A similar mechanism to produce non-isotropic illumination is considered for FU Orionis stars by Bell & Chick (1997).

This paper presents new imaging and spectroscopic data on the Cha IRN to learn more about this fascinating object.

*Send offprint requests to*: M. Feldt (mfeldt@astro.uni-jena.de)

⋆ Based on observations collected at the European Southern Observatory, La Silla, Chile

⋆⋆ based on observations with ISO, an ESA project with instruments funded by ESA Member States (especially the PI countries: France, Germany, the Netherlands and the United Kingdom) with the participation of ISAS and NASA

**Table 1.** Log of observations

| Date | Tel./Instr. | $\lambda$ | Ref. Star |
|---|---|---|---|
| 1992 Feb. | 3.6 m/TIMMI | 10 $\mu$m | HR4671 |
| 1992 August | NTT/SHARP | 2.20 $\mu$m (K) | Sgr 9 |
| 1994 April | NTT/IRSPEC | 2.30 – 2.36$\mu$m | HR5787 |
| 1994 April | NTT/IRSPEC | 3.00 – 4.03$\mu$m | HR5787 |
| 1994 April | NTT/IRSPEC | 4.59 – 4.86$\mu$m | HR5787 |
| 1995 Nov. | 2.2 m/IRAC2b | 1.25 $\mu$m (J) | HD18847 |
| 1995 Nov. | 2.2 m/IRAC2b | 1.65 $\mu$m (H) | HD18847 |
| 1995 Nov. | 2.2 m/IRAC2b | 2.11 $\mu$m (K') | HD18847 |
| 1996 Feb. | ISO/ISOPHOT-S | 2.5-11.6$\mu$m | |

In Sect. 2 we describe the observations and the data reduction process. This covers the near-infrared images, obtained with IRAC2b at ESO's 2.2 m telescope, speckle data taken at the NTT using SHARP I, and spectroscopic data obtained using IRSPEC at ESO's NTT and ISOPHOT-S. In Sect. 3 we use the imaging data to discuss morphological properties of the nebula. These data support the hypothesis that a very young binary system is located inside the Cha IRN. Additionally, we derive the grain composition of the surrounding dust from the spectra. Here we found indications for water and, only very marginally, ammonia ice together with clear evidence for CO and $CO_2$. Features from PAH emission are completely lacking and the silicate absorption band at 10 $\mu$m is not detected. Finally in Sect. 4, we present the results obtained using our radiative transfer model to fit the SED, the IR spectra and the mid-infrared appearance. Combined with our new NIR images of Cha IRN, this approach results in a self-consistent model of the source.

## 2. Observations and data reduction

### *2.1. IR spectra*

Infrared spectra of the Cha IRN were obtained in April 1994 using the Infrared Spectrometer IRSPEC on ESO's New Technology Telescope (NTT) on La Silla, Chile. A log of all observations is shown in Table 1. IRSPEC is described in Gredel & Weilenmann (1992). Grating 1 was used for all spectra, 2nd order for the 2.3$\mu$m range, 1st order for the other ranges. For wavelength calibration, an internal spectral lamp was used. For sky subtraction, a second spectrum of the object shifted a few arc-seconds along the slit was obtained. HR5787 served as the standard star. Data reduction followed the IRSPEC context of ESO's MIDAS data reduction package. Integration times were different for each spectral range and for object and standard star, but always chosen to result in similar count numbers and not to saturate the detector.

### *2.2. JHK imaging*

Imaging of the Cha IRN was performed in November 1995 using IRAC2b on ESO's 2.2 m telescope on La Silla, Chile. The use of objective B of IRAC2b resulted in a scale of 0.27″ per pixel. For bad pixel correction and sky subtraction, a mosaic mode was chosen. In each wavelength, five integrations were performed, four with the object in a different quadrant of the detector, and one with the object near its centre. A sky image was obtained by taking the median of this cube of five frames. Bad pixels were first corrected by replacing their signal with one from a frame with the object at a different position, then by conventional bad pixel correction using a seek & correct algorithm. This procedure resulted in a total integration time of 10 minutes on the object in each band, with smaller integration times in adjacent areas. Fig. 1 shows a region of the resulting K' mosaic. For flux calibration, similar images of HD18847 were taken. Additionally, we incorporate a K-band high-resolution image obtained by speckle interferometry (Stecklum et al. 1993).

### *2.3. 10 $\mu$m imaging*

The 10 $\mu$m imaging was performed in 1994 using TIMMI at ESO's 3.6 m telescope on La Silla/Chile (Käufl et al. 1992). The pixel scale is 0.3″. The profile shown in Fig. 6 is the result of 750 stacked frames. The detection limit in the image is 0.6 Jy. With this sensitivity, we do not detect any significant deviation from the point spread function, i.e. the source appears unresolved at the nominal resolution of 1″.

### *2.4. ISO data*

These observations were carried out using the spectrophotometer subsystem of ISO's imaging photo-polarimeter ISOPHOT. A detailed description of this instrument can be found in Lemke et al. (1996). The data processing was done using the PHT Interactive Analysis (PIA) software made available by the ISOPHOT Data Centre of the Max Planck Institute for Astronomy, Heidelberg[1]. The flux of the ISO spectra differs from the IRSPEC and the IRAS data by a factor of 2.2. Two explanations for this deviation can be thought of: First, the satellite was pointed at the nominal position of IRAS11072-7727. This means, that with the ISOPHOT field of view of 24″×24″, only the eastern half of the source has been measured. Secondly, the absolute photometric calibration of ISOPHOT may not yet be very accurate. In Fig. 5, the ISO data have been multiplied by a factor of 2.2 to match the fluxes of IRAS and IRSPEC data.

## 3. Discussion

In this section, we use the near-infrared imaging data to discuss the morphological properties of the infrared nebula. First, conclusions are drawn from the visual appearance by interpreting the different features as astrophysical phenomena. This indicates an outflow and the principal, already well-known orientation of the disk. Going further, we use colour indices and the

[1] PIA is a joint development by the ESA Astrophysics Division and the ISOPHOT Consortium led by the Max Planck Institute for Astronomy (MPIA), Heidelberg. Contributing ISOPHOT Consortium institutes are DIAS, RAL, AIP, MPIK, and MPIA.

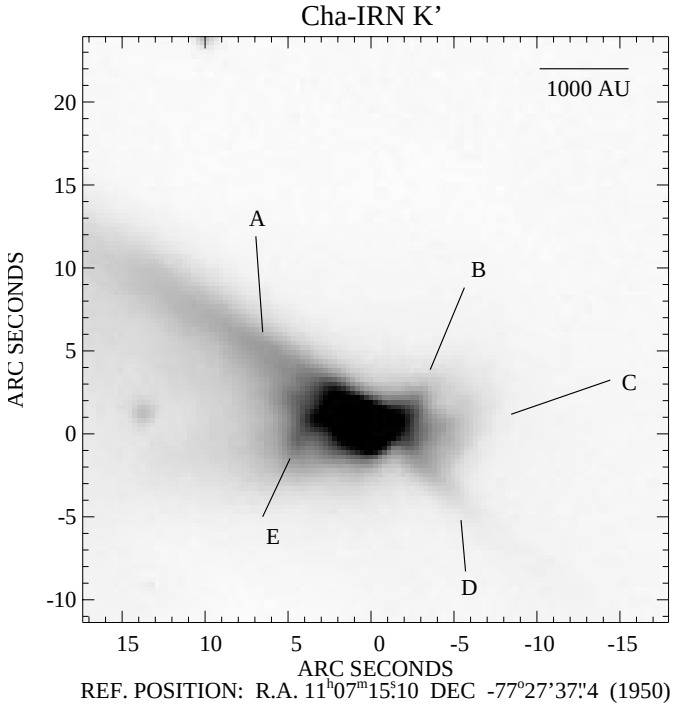


**Fig. 1.** K' image of the Cha IRN. The linear grey scale ranges from 0 to 4 mJy per square arc second. The features A-E are mentioned in the text.

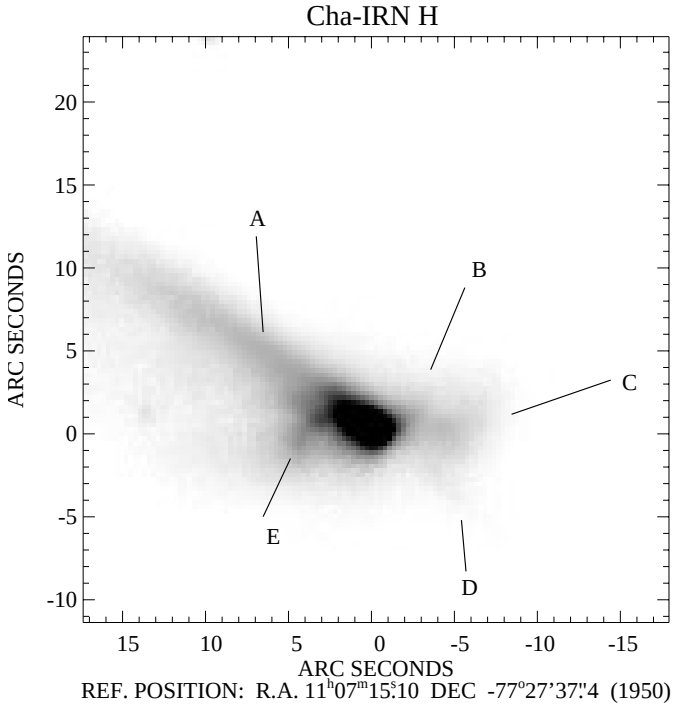


**Fig. 2.** H Image of Cha IRN. Same grey scale and feature labels as in Fig. 1

wavelength-dependent position of the object to confirm the details of the geometry. The second part of the section deals with the spectra and the derivation of the dust composition therefrom.

### *3.1. Disk and outflow*

In Figs. 1 through 3, the NIR images of the IR nebula can be seen. They all show some common features: From the bright knot at the reference position, the nebula stretches to the east and, much weaker, to the west. The general features of the Cha IRN are already well known with bright elongated structures to the northeast (feature A), the northwest (B) and the southwest (D). These bright lobes are generally believed to be the brightened rims of parabolic cavities, cleared by outflow activity (e.g. Gledhill et al. 1996). These cavities point to the east and to the west. The southeastern rim is then missing, probably due to foreground extinction. The parabolic cavities exhibit a position angle of 87°, which would in turn point towards a molecular disk at P.A. 177°. However, the polarization studies by Ageorges et al. (1996) and Gledhill et al. (1996) show an aligned polarization vector pattern at P.A. 160° towards the central bright knot. This indicates a tilted inner part of the disk, an effect which according to Gledhill et al. (1996) might be caused by tidal forces from a young binary system inside.

In Fig. 1 through 3, two more features can be seen: A tail-like structure pointing from the bright knot to the west and turning north (Feature C) and another tail, pointing east and turning south (E). Features (C) and (E) are best visible at the shorter NIR wavelengths, which is obvious from the J-band image shown in Fig. 3. Fig. 4 shows the contours of the high-resolution speckle image, superimposed on the grey-scale image from Fig. 1. These contours reveal some inner structure of the bright knot. Apart from the bright peak itself, the highest contours trace a structure which seems to be the inner origin of feature E. Also, the upper rim of the contour pattern is obviously the inner part of the bright rim marked as feature (A). The beginning of the missing lower rim can marginally be seen at the southern edge of the pattern. This indicates that foreground extinction already starts shortly south of the main peak. West of the bright knot, almost no contour lines are visible. Only a very weak structure at position (-2″,+1″) is visible. This feature shows two elongations which could be interpreted as the origins of features (B) and (C). If this is indeed the case, then features (C) and (E) meet at the approximate position (0″,+0.6″) with P.A. 84°. Altogether (C) and (E) form an S-shaped feature and could be interpreted as the signature of a bipolar outflow. The curvature indicates the presence of a second stellar component in the system. Such a binary can provide the bending of the two lobes, e.g. by causing a tilt in the inner disk through tidal forces. The disk would then start to precess and force the outflow to follow the motion of its polar axis. This scenario is also consistent with the presence of a tilted inner disk mentioned above. A second explanation can be thought of by assuming the companion star itself to be the source of the outflow. In this case the curvature could be caused by the orbital motion (provided that the orbital velocity is of the same order of magnitude as the outflow velocity) like in the model for T Tau by van Langevelde et al. (1994). In both cases, the main polar axis is defined by the large-scale

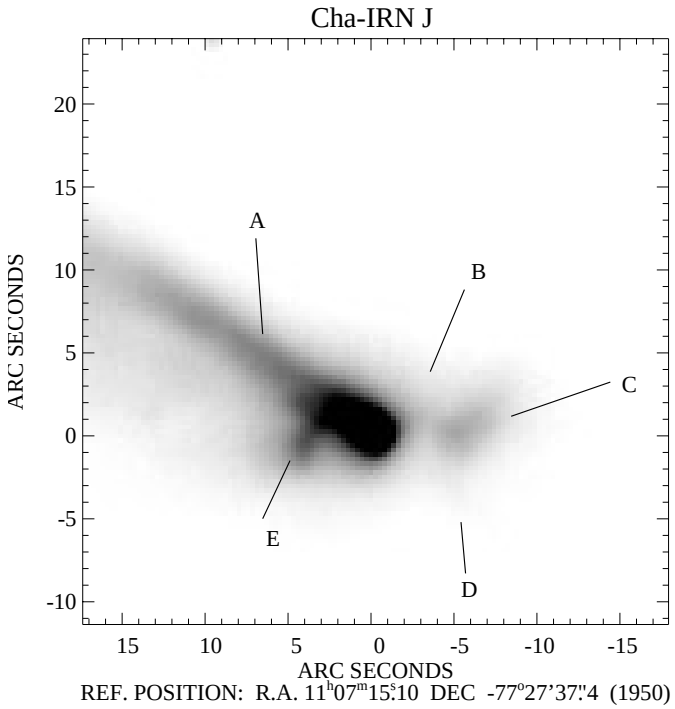


**Fig. 3.** J Image of Cha IRN. In this band, the features E and C are best visible.

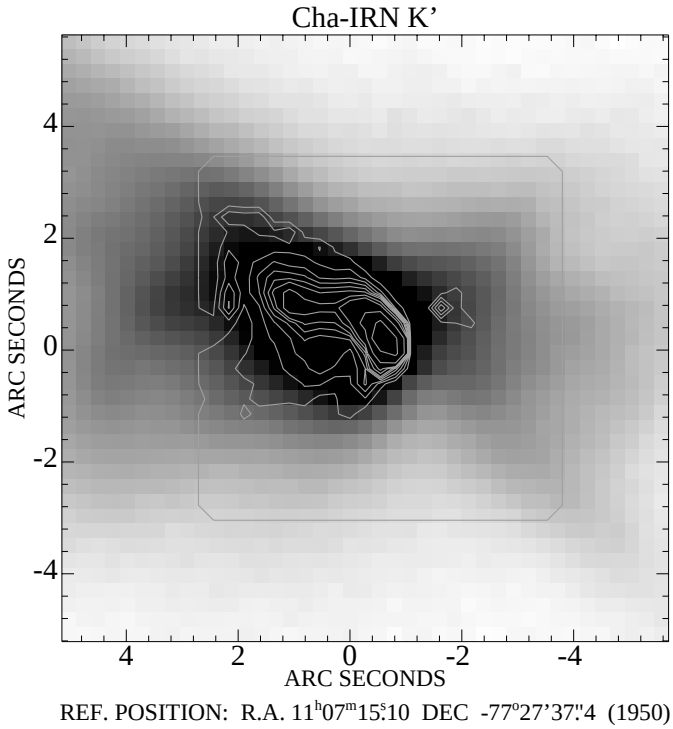


**Fig. 4.** Central part of the K image, overlaid with contours of the high-resolution speckle image. Contour levels are 1,2,3,4,5,6,8,10,20, and 40 times 0.12 Jy per square arc second.

molecular disk at P.A. 177°, which is in agreement with the bipolar cavities and probably with the orbital plane of the binary system. As a counterpoint to this line of reasoning it has to be mentioned that no apparent molecular outflow from Cha IRN has been found up to now, despite a CO search with the SEST by Ageorges (1997, priv. comm.). From Figs. 1, 2, and 3, we computed the colour indices of the Cha IRN. The J, H, and K' images have been aligned using the star at (+9″,+25″) (see the northern edge of Fig. 1) as a reference point. The reddest parts of the images are the bright knot itself and the two rims of the western outflow cavity. The knot has indices of $J$–$H = 1.0$ mag and $H$–$K = 1.1$ mag, whereas the western rims show indices around $J$–$H \approx 0.7$ mag and $H$–$K \approx 1.0$ mag. In fact, the western rims, denoted as features (B) and (D), are hardly visible in Figs. 2 and 3. East of the bright knot, colour indices range up to only $J$–$H = 0.35$ mag and $H$–$K = 0.5$ mag. This leads to the conclusion that the disk is inclined such that the western lobes are viewed through the outer parts of the disk plane.

Using the distance of 190 pc towards the object and the fact that all the previous investigations indicate a disk inclination of 70°, we can now derive the linear size of the disk: Since the western lobes appear strongly reddened out to a distance of 680 AU (and thus appear "covered" by the disk), we compute its radius to be at least 2000 AU. This value is larger than the 1000 AU obtained by Ageorges et al. (1996) and the 1400 AU assumed by Cohen & Schwartz (1984) and Gledhill et al. (1996). However, the latter two sizes were based on a distance estimate of 140 pc.

Another fact can be utilized to confirm the spatial orientation of the disk: If we calculate the centroid position of the bright knot, we see that it is different in the three bands. The position in H is shifted by ($\Delta\alpha$=-0.3″, $\Delta\delta$=-0.08″) with respect to J, in K by ($\Delta\alpha$=-0.5″, $\Delta\delta$=-0.08″). This positional shift between wavelengths is a classical indicator for reflection at cavity walls emerging from an inclined disk (see, e.g., Stecklum et al. (1997) for GGD 27 or Close et al. (1997) for HL Tau). The small shifts in declination point to a very small bending angle out of the north south plane. From these measurements, the position angle of the disk plane would be between 170° and 180°. This indicates that the large-scale disk (not the tilted, inner one) is responsible for the effect of the position shift between wavelengths. The direction of the shifts also confirms that we are facing the eastern surface of the disk, the inclination therefore obscuring and thus reddening the western cavity walls. However, the errors in these measurements are of the order $\pm$0.3″, so this can only be seen as a principal indicator. The fact that we do not see the small-scale inner disk with this method is consistent with Gledhill et al. (1996), who assume this part to be unresolvable by their observations. This means that the inner disk should not show any direct effect in our images.

### *3.2. IR spectra*

We will now discuss the infrared spectra taken with IRAS, ISO, and IRSPEC. The combined spectra of the Cha IRN are shown in Fig. 5. Several features can be identified in them, the most obvious being the $H_2O$ ice band near 3.1 $\mu$m. The optical depth of 3.3 at the centre of this feature makes it one of the most

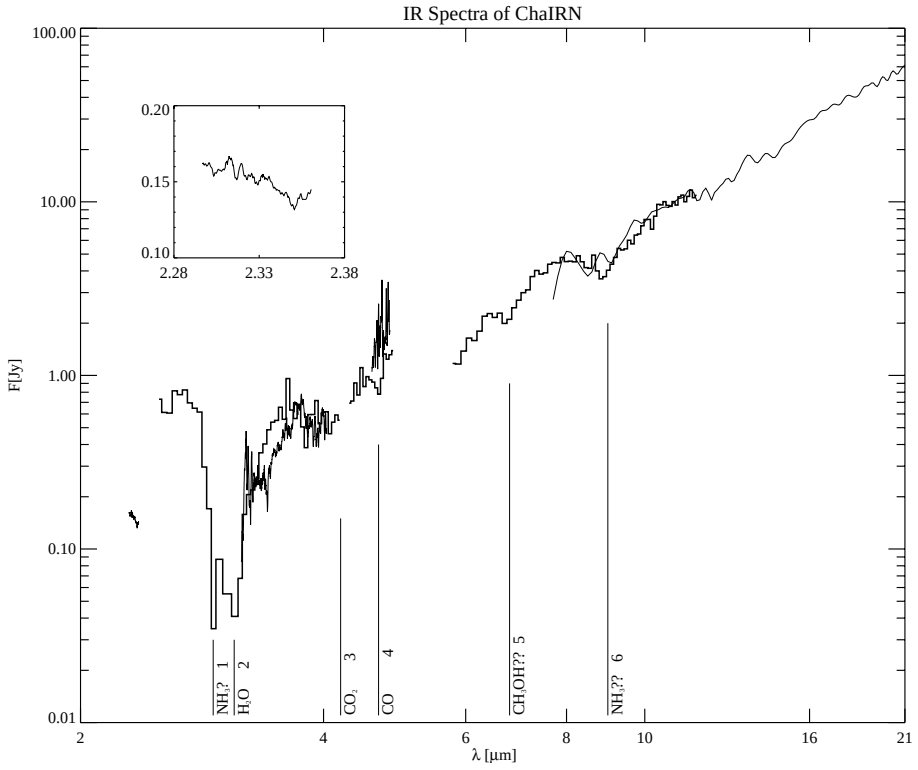


**Fig. 5.** IR spectra of Cha IRN. The IRSPEC data range from 2.2–5 $\mu$m and are denoted by a solid line. The thick steps denote the ISO data. From 8–20 $\mu$m the IRAS LRS-Spectrum is shown for comparison. The inset gives an enlarged view of the 2.3 $\mu$m region of the IRSPEC data.

**Table 2.** Identified absorption features, line data and derived column densities

| ID | $\lambda$ [$\mu$m] | Designation | $\Delta\nu$ [cm$^{-1}$] | $\tau$ | A [cm$\cdot$ molecules$^{-1}$] | $N$ [cm$^{-2}$] |
|---|---|---|---|---|---|---|
| 1 | 2.9 | $NH_3$ | 52.6 | 1.7 | $1.1{\cdot}10^{-17}$[a] | $8.1{\cdot}10^{18}$ |
| 2 | 3.1 | $H_2O$ | 199.3 | 3.3 | $2.0{\cdot}10^{-16}$[b] | $3.3{\cdot}10^{18}$ |
| 3 | 4.2 | $CO_2$ | 14.27 | 1.7 | $3.3{\cdot}10^{-17}$[b] | $3.3{\cdot}10^{17}$ |
| 4 | 4.7 | CO | 24.11 | 0.42 | $1.1{\cdot}10^{-17}$[b] | $9.2{\cdot}10^{17}$ |
| 5 | 6.8 | $CH_3OH$??, unknown | 38.1 | 0.26 | | |
| 6 | 8.9 | $NH_3$?? | 17.4 | 0.26 | $1.7{\cdot}10^{-17}$[a] | $2.6{\cdot}10^{17}$ |

[a] From d'Hendecourt & Allamandola (1986)
[b] From Gerakines et al. (1995)

prominent ones known in protostellar spectra, similar to the one in AFGL 2136 (Kastner & Weintraub 1996) and W3-IRS5 (Smith et al. 1989). The long wavelength wing of the feature is slightly different in the IRSPEC and ISOPHOT spectra. The IRSPEC data indicate a more pronounced wing. Characteristics of the features are summarized in Table 2. The line centre, optical depth and full width half maxima have been determined by fitting a Gaussian profile to each absorption line and using the parameters from the fit. For continuum subtraction, quadratic baselines were fitted to the immediate neighbourhood of the features. In case of the 2.9 $\mu$m $NH_3$ feature, the fit of the 3.1 $\mu$m $H_2O$ was subtracted as background before fitting the line. All features were identified in the ISO data, the results of IRSPEC being too noisy to deliver useful results. The IRSPEC data do, however, confirm the general course of the spectrum. The IRAS data also show no features, apart from a slightly noise contaminated confirmation of the 8.9 $\mu$m feature.

In Table 2 we also give the derived column densities $N$ for each molecular species. The latter are calculated using the relation $N \approx \frac{\tau \cdot \Delta\nu}{A}$, where $A$ is the integrated absorbance, $\Delta\nu$ the measured line width (FWHM), and $\tau$ the optical depth of the line. The ISO data show a narrow secondary dip within the $H_2O$ absorption feature. Decomposing the two features and measuring their parameters yields the values given in Table 2.

These data indicate that ammonia is approximately 2.5 times more abundant than water, a fact which seems rather unlikely. Due to the complicated line subtraction process and the fact that the feature shows up in essentially only one single ISO data point, this result should be viewed with a healthy amount of suspicion. More so, because the 8.9 $\mu$m feature, if attributed to ammonia as well, would yield a column density of only $N_{\mathrm{NH_3}} = 2.6 \cdot 10^{17}$ cm$^{-2}$, which makes only 8% of the water abundance. To a limited extent, the inconsistency between the two column densities for ammonia could be explained by the

fact that radiation with wavelength 8.9 $\mu$m is probing deeper into the edge-on disk, while at 3 $\mu$m we observe mostly photons leaking out from the poles (Pendleton et al. 1990). If this is true, then ammonia must be more abundant (compared to water) in the ambient cloud material, than in the disk itself. The origin of the 8.9 $\mu$m feature is, however, uncertain altogether. It might also be due to methanol or a forbidden line of Ar III gas.

The feature at 6.8 $\mu$m is clearly visible. However, it is still unclear, to which molecular species it can be attributed. Possible explanations include methanol, $NH_4^+$ and a blend of several different absorption components (Henning 1996). We do not derive abundances for methanol here, since we do not detect absorption features at 3.4 $\mu$m, 3.5 $\mu$m, 9.7 $\mu$m, or 14.2 $\mu$m. The other two identified features are at 4.2 $\mu$m and 4.7 $\mu$m, indicating the presence of $CO_2$ and CO. The derived abundance ratios relative to water are consistent with the ratios for which the absorbance strengths were determined. The latter are, however, anyhow only weakly dependent on the mixture (Gerakines et al. 1995). To summarize the spectral data, we detected a grain mixture of

$$H_2O{:}CO{:}CO_2{:}NH_3 = 100 : 28 : 10 : 8,$$

with the value for $NH_3$ being rather uncertain.

Despite the disk is seen nearly edge-on, we do not find any silicate absorption feature at 10 $\mu$m. Therefore, the silicate abundance in the disk seems to be unusually low. Silicate absorption in the spectra of young stellar objects usually appears in form of a wide, structureless feature peaking at 9.7 $\mu$m (Jäger et al. 1994). In comets and Vega-type stars, silicate features are found that have an additional peak at 11.2 $\mu$m, which indicates the presence of crystalline silicates. As this shows that the actual position of the silicate feature might appear shifted by a considerable amount, one might now be tempted to speculate that we *did* detect some silicate absorption in form of the 8.9 $\mu$m feature. However, we do not ascribe this feature to an exotic species of silicates and do not take it as an indication of any weak silicate absorption at all.

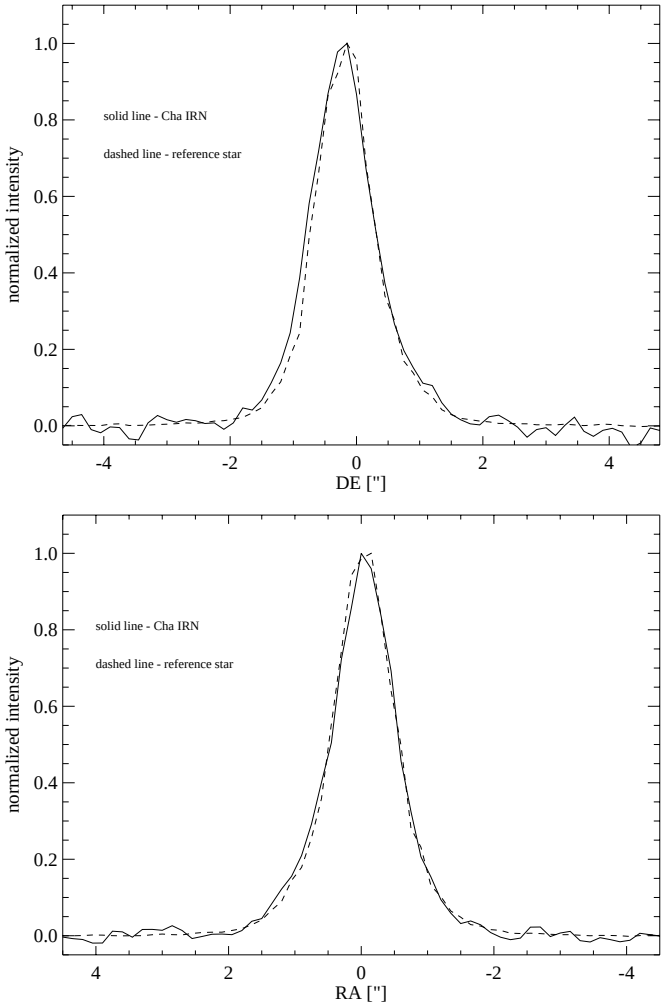


**Fig. 6.** The profiles of Cha IRN at 10$\mu$m compared to a point source. Only in Declination the Cha IRN appears to be slightly resolved, i.e. larger than the beam size of 1”

## 4. Towards a self-consistent model of Cha IRN

In this section, we will discuss the results of a radiative transfer model which was used to construct a self consistent model of the Cha IRN star/disk system. Before we present the results, we will summarize the observational constraints and give a short outline of the radiative transfer model.

### *4.1. Constraints on the model*

By modelling the radiative transfer through the disk, it is also possible to determine the geometry of the star/disk system. To achieve this goal, it is necessary to fit the model spectrum to a wavelength range as wide as possible. Additionally, it is necessary to introduce as many observational constraints to the model as possible. From the IR spectra, we learn that there is mainly water, CO, and $CO_2$ ice on the grains. The optical depth of the 3.1$\mu$m ice feature of $\tau = 3.3$ points to a visual extinction of $A_V \approx 70$ mag (Tanaka et al. 1990). According to Mathis (1990), this implies a K-extinction of $A_K \approx 6.3$ mag. Together with the distance modulus of 6.4 mag, we get a total extinction in K of around 12.7 mag. As we cannot detect the central object with our limiting magnitude of K=15 mag, this means it must at least have an absolute magnitude of $M_K$=2.3 mag. If this was to be attributed to a single main-sequence object, it would have to be of a spectral type later than F. However, such stars do not posses sufficient luminosity to explain the observed radiation from the whole object, which in turn would point to another source of radiation, e.g. active accretion from the disk. Alternatively, if the source is “beaming out” its radiation into the outflow lobes, as suggested by the polarized source model of Gledhill et al. (1996), the central object might well be considerably brighter. This would imply that the visual extinction towards the central object can be much higher than the above estimate (see the discussion of the radiative transfer model in the next section). Also, considering a binary system might change this estimate altogether.

**Table 3.** Parameters used in the model fit to the SED

| | |
|---|---|
| **Central Object:** | |
| Luminosity: | $L = 170 \mathrm{L}_\odot$ |
| Temperature: | $T = 7000K$ |
| Distance: | $D = 190$ pc |
| **Disk Structure:** | |
| Density distr.: | $\rho(r) \sim r^{-1} (r \leq 60\,\mathrm{AU})$ |
| | $\rho(r) \sim r^{0} (r > 60\,\mathrm{AU})$ |
| Outer radius: | $\mathrm{R_{out}} = 2000$ AU |
| Inner radius: | $\mathrm{R_{in}} = 5$ AU |
| Opening angle: | $45^\circ$ |
| Inclination: | $68^\circ$ |
| **Dust Properties:** | |
| Size distribution: | $a = 0.01 - 0.4\,\mu$m |
| | $N(a) \sim a^{-3.5}$(MRN) |
| Silicate / Carbon ratio: | Si:C = 1:4 |
| Optical data: | Draine & Lee (1984) |
| Optical depth: | $\tau_{550} = 120$ |

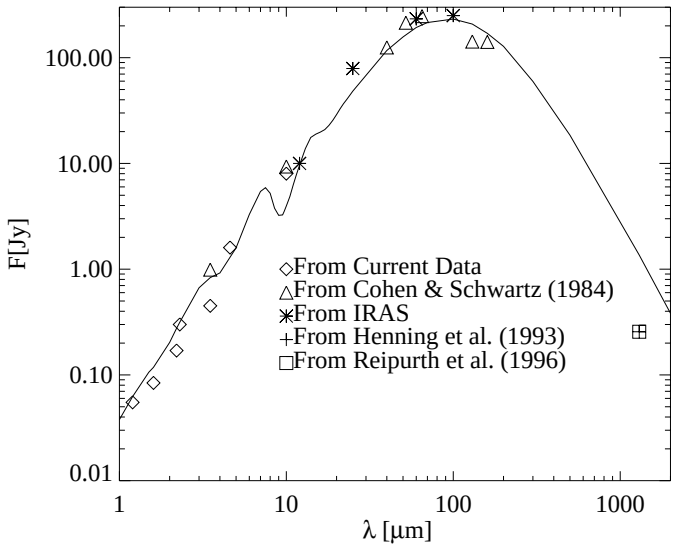


**Fig. 7.** The spectral energy distribution of Cha IRN (symbols) and the model fit to it. The solid line gives the total flux from the object as calculated from the model. Beam size effects do not apply except at 3.5 $\mu$m, where the beam-corrected model flux is 0.2 Jy below the total flux.

A further hint towards the structure of Cha IRN is the point-like appearance at 10 $\mu$m (see Fig. 6) which means that the warm dust is concentrated close to the central object. This is a fact, against which the result of a radiation transfer calculation has to be checked.

As stated in Sect. 3.1, we estimate the disk's radius to be of the order of 2000 AU. The fact that we do not detect any silicate feature in the spectrum might have two consequences for the model: Either the silicate abundance is unusually low or some kind of geometrical effect provides a cancelling mechanism for the expected 10 $\mu$m feature.

### *4.2. The radiative transfer code*

The code used for fitting the spectral energy distribution and constraining the geometry of the dust configuration was developed by Manske et al. (1997) and is based on a method given by and described at length in Men'shchikov & Henning (1997). The main approximation used in this code is that, in spite of the flared disk geometry, the density distribution depends on the radial coordinate only. In addition, mean intensities and temperatures are self-consistently calculated for points in the disk's mid-plane and at its upper and lower conical surfaces only. The disk itself is part of a sphere with removed polar cones. Extensive explanations of the code and its strategy for solving the radiative transfer problem can be found in the two papers mentioned above.

### *4.3. The resulting model*

In Fig. 7, we show the result of our model calculations compared to the spectral energy distribution of Cha IRN. The parameters used for the model are given in Table 3.

The fit confirms the basic assumptions on the geometry of the system: A large-scale disk with a radius of 2000 AU, viewed at an inclination of 68°, i.e. 22° out of the plane of sight very well reproduces the spectral energy distribution. The most striking features of the model are:

– The unusually low silicate fraction in the dust composition. This is of course a result from the fact that no silicate feature is observed. As we could not completely reproduce a spectrum without a silicate feature by varying the geometry, we had to reduce the silicate-to-carbon ratio to 1:4. However, our model is not able to take all possible geometric effects into account: The density is independent from the distance from the disk's mid-plane. In reality however, the parts further from the mid-plane might exhibit lower density and thus lower optical depth. As we are looking at the central object almost along the disk's surface, silicate emission from the optically thin surface layers might "fill" the absorption feature. We should note that a similar spectral behaviour (no silicate feature) was found by Koresko et al. (1997) in case of Haro 6-10.
– The high luminosity of the central object(s), that by far exceeds the observed luminosity of 14.4 $\mathrm{L}_\odot$ from Cohen & Schwartz (1984). Of course the highly non-spherically symmetric nature of the object easily explains the difference, yet this might be another hint that more than one central star contributes to the energy supply.
– In the near-infrared region, we only considered the light from the inner 2″. In order to reproduce this part of the SED, we had to exclude scattering at the conical surfaces of the disk. Otherwise, the near-infrared brightness of the model would be orders of magnitude larger. This could mean that the disk surface is protected from direct starlight. Another possibility is the blocking of scattered NIR light by a slab of foreground extinction (see Ageorges et al. 1996).

Additionally, the model predicts an intensity distribution at 10 $\mu$m with a FWHM of only 0.12″ in right ascension and 0.19″ in declination. When observed with a 1″ beam, the result in declination should have a FWHM 0.02″ larger than the beam. This of course cannot be seen with a pixel size of 0.3″. However we do see a slight elongation by one pixel in declination in Fig. 6. Fig. 6 shows the measured intensity distribution of Cha IRN at 10 $\mu$m. In this figure, the source appears unresolved. This means that we can set an upper limit of 1″ for the size, which is in good agreement with the model prediction.

## 5. Conclusions

The imaging data presented in this paper revealed an S-shaped feature emerging from the central part of Cha IRN. This feature may be interpreted as a bended outflow. The necessity for a "bending" mechanism points towards the presence of a binary system inside the nebula. Additionally, our data confirmed earlier assumptions on the overall geometry of the system such as inclination and position angle of the large-scale molecular disk. spectroscopically, we detected one of the most prominent $H_2O$ features as well as indications for CO, $CO_2$ and possibly $NH_3$. No silicate absorption feature is found in the spectra, this indicates either an unusually low fraction of this molecular species or the presence of some cancelling mechanism for the absorption feature. The radiative transfer calculations show that the results on geometry and dust composition are compatible with the spectral energy distribution, if three prerequisites are met: The silicate-to-carbon-ratio has to be assumed to be 1:4, the central object has to be very luminous with $L = 170 L_\odot$ and scattering of near-infrared light on the disk's surface has to be excluded somehow.

*Acknowledgements.* Part of this work was supported by the German *Deutsche Forschungsgemeinschaft, DFG* project number Ts 17/2–1. We also acknowledge support through the Verbundforschung Astronomie und Astrophysik, contract No. 50 OR 9414 9 for funding the ISO part of the project. The authors acknowledge the service of the *Centre de Données astronomiques de Strasbourg* , which has made available the Hipparcos Data through the world wide web (http://cdsweb.u-strasbg.fr/cgi-bin/myqcat3?hipparcos). We also acknowledge the service of the IRAS SOFTWARE TELESCOPE (IST) system in Groningen, which made available the IRAS spectra of Cha IRN (mailto:irasman@sron.rug.nl).

## References

Ageorges N., Fischer O., Stecklum B., Eckart A., Henning Th., 1996, ApJ 463, L101
Bell K.R., Chick K.M., 1997, in: Reipurth B., Bertout C. (eds.) Herbig Haro Flows and the Birth of Low Mass Stars. IAU Symp. No. 182, Kluwer, Dordrecht, p.407
Cohen M., Schwartz R.D., 1984, AJ 89, 277
Close L.M., Laird M., Roddier F. et al., 1997, ApJ 478, 766
Draine B.T., Lee H.M., 1984, ApJ 285, 89
Gerakines P.A., Schutte W.A., Greenberg J.M., van Dishoeck E.F., 1995, A&A 296, 810
Gledhill T.M., Chrysostomou A., Hough J.H., 1996, MNRAS 282, 1418
Gredel R., Weilenmann U., 1992, Msngr 70, 62
d'Hendecourt L.B., Allamandola L.J., 1986, A&AS 64, 453
Henning Th., 1996, in: Greenberg J.M. (ed.) The Cosmic Dust Connection, Kluwer, Dordrecht, p. 399
Henning Th., Pfau W., Zinnecker H., Prusti T., 1993, A&A 276, 129
Jäger C., Mutschke H., Begemann B., Dorschner J., Henning Th., 1994, A&A 292, 641
Kastner J.H., Weintraub D.A., 1996, ApJ 466, L103
Käufl H.U., Jouan R., Lagage P. O., Masse P., Mestreau P., Tarrius A., 1992, Msngr 70, 67
Koresko C.D., Herbst T.M., Leinert Ch., 1997, ApJ 480, 741
Lemke D., Klaas U., Abolins J. et al, 1996, A&A, 315, L64
Manske V., Henning Th., Men'shchikov A.B., 1997, A&A, in press
Mathis J.S., 1990, ARA&A, 28, 37
Men'shchikov A.B., Henning Th., 1997, A&A 318, 879
Pendleton Y.J., Tielens A.G.G.M., Werner M.W., 1990, ApJ 349, 107
Reipurth B., Nyman L.A., Chini R., 1996, A&A 314, 258
Rydgren A.E., 1980, AJ 85, 444
Schwartz R.D., Henize K.G., 1983, AJ 88, 1665
Smith R.G., Sellgren K., Tokunaga A.T., 1989, ApJ 344, 413
Stecklum B., Henning Th., Eckart A., Hofmann R., 1993, Infrared. Phys. Technol. 35, 487
Stecklum B., Feldt M., Richichi A., Calamai G., Lagage P.O., 1997, ApJ 479, 339
Tanaka M., Sato S., Nagata T., Yamamoto T., 1990, ApJ 352, 724
van Langevelde H.J., van Dishoeck E.F., van der Werf P.P., Blake G.A, 1994, A&A 287, L25